RadioGraphics

Informatics in Radiology (*info*RAD)

New Tools for Computer Assistance in Thoracic CT Part 1. Functional Analysis of Lungs, Lung Lobes, and Bronchopulmonary Segments[1]

Jan-Martin Kuhnigk, Dipl CS • Volker Dicken, PhD • Stephan Zidowitz, PhD • Lars Bornemann, Dipl CS • Bernd Kuemmerlen, Dipl Phys • Stefan Krass, PhD • Heinz-Otto Peitgen, PhD • Silja Yuval • Hans-Holger Jend, MD • Wigbert S. Rau, MD • Tobias Achenbach, MD

Owing to the rapid development of scanner technology, thoracic computed tomography (CT) offers new possibilities but also faces enormous challenges with respect to the quality of computer-assisted diagnosis and therapy planning. In the framework of the Virtual Institute for Computer Assistance in Clinical Radiology cooperative research project, a prototypical software application was developed to assist the radiologist in functional analysis of thoracic CT data. By identifying the anatomic compartments of the lungs, the software application enables assessment of established functional CT parameters for each individual lung, pulmonary lobe, and pulmonary segment. Such region-based assessment allows a more localized diagnosis of lung diseases such as emphysema and more accurate estimation of regional lung function from CT data. With close cooperation between computer scientists and radiologists, the software application was tested and optimized to achieve a high degree of usability. Several clinical studies were carried out, the results of which indicated that the software application improves quantification in diagnosis, therapy planning, and therapy monitoring with respect to accuracy and time required.

Abbreviations: FEV_1 = forced expiratory volume in 1 second, 3D = three-dimensional

RadioGraphics 2005; 25:525–536 • **Published online** 10.1148/rg.252045070 • **Content Codes:** CH CT HP

[1]From the MeVis Center for Medical Diagnostic Systems and Visualization, Universitaetsallee 29, 28359 Bremen, Germany (J.M.K., V.D., S.Z., L.B., B.K., S.K., H.O.P.); the Center for Radiology, Hospital Bremen—East, Germany (S.Y., H.H.J.); the Department of Diagnostic Radiology, University Hospital Giessen, Germany (W.S.R.); and the Department of Radiology, University Mainz, Germany (T.A.). Presented as an *info*RAD exhibit at the 2003 RSNA Scientific Assembly. Received April 7, 2004; revision requested June 30 and received August 20; accepted September 10. Supported by grant 01EZ0010 from the German Federal Ministry of Education and Research. All authors have no financial relationships to disclose. **Address correspondence to** J.M.K. (e-mail: *kuhnigk@mevis.de*).

See Bornemann et al in the May 2005 issue of *RadioGraphics* for Part 2 of this two-part series of articles.

Introduction

The advantages of three-dimensional (3D) reconstruction and visualization for pulmonary computed tomography (CT) were outlined by Rubin et al (1) a decade ago. Since that time, there has been enormous progress in image quality, mainly due to the advent of multidetector CT scanners. The introduction of four-section CT was a breakthrough for thoracic CT because this scanner technology allowed, for the first time, the performance of isotropic CT volume scans in a single breath hold (2). Comparable substantial progress is now being made in the field of cardiac CT by the 16-section scanner technology (3). Particularly in thoracic CT, this improvement in spatial resolution results in a large number of sections, which are difficult for a radiologist to read within an acceptable time. On the other hand, the resolution achieved in thoracic CT allows the application of high-precision 3D image analysis tools to thoracic CT data.

The progress in image quality has an impact on a number of applications in thoracic CT, for example, evaluation of the tracheobronchial tree, assessment of diffuse lung disease, and more accurate prediction of pulmonary nodule volume and growth, as described in reference 4. These improvements in imaging of airways, pulmonary and systemic vessels, and lung nodules combined with the application of image processing techniques yield substantial progress in diagnostic imaging of the lung (5). A collection of various lung diseases imaged with multidetector CT is shown in reference 6.

Because of the rapid development of scanner technology, thoracic CT offers completely new possibilities but also faces enormous challenges concerning the quality of computer-assisted diagnosis and therapy planning. In the framework of the German VICORA (Virtual Institute for Computer Assistance in Clinical Radiology) research collaboration (7,8), applications were developed that offer solutions in the following areas of thoracic CT: *(a)* improved CT-based functional diagnosis with quantitative CT parameters for each lobe and segment and methods for quantification and classification of emphysema, *(b)* examination of large data sets by means of anatomically adequate 3D visualization techniques, and *(c)* follow-up of tumor therapy by volumetric quantification of tumors and temporal registration. These functionalities are implemented in two new prototypical applications: MeVisPULMO for functional analysis of pulmonary CT data and PulmoTREAT for allowing therapy monitoring in metastatic lung disease.

In this article, we discuss the motivation for the development of MeVisPULMO, describe the use of MeVisPULMO, and provide the results of evaluations of MeVisPULMO. The PulmoTREAT application will be presented in the next issue of *RadioGraphics*.

TAKE-HOME POINTS

- The prototypical software application MeVisPULMO allows convenient quantitative 3D analysis of pulmonary CT scans.
- Volumes and CT parameters such as mean attenuation or pixel index can be extracted specifically for each lung, pulmonary lobe, or pulmonary segment for localized assessment of restrictive and obstructive lung diseases.
- In cases of lobar resection surgery, postoperative lung function can be estimated from results of lung function tests and the novel CT-based image analysis technique alone.
- To allow seamless integration into a clinical setting, the work flow of the application is separated into a fully automated preprocessing procedure, in which the time-consuming image processing tasks are performed, and an evaluation and reporting step.

Motivation

Recent multidetector CT devices allow improved and more detailed imaging of lung tissue. Examinations of the lung parenchyma are frequently performed with a section thickness of 1 mm and approximately isotropic voxels, resulting in a large number of images. Imaging of patients with lung emphysema typically produces data sets with 300 or more sections. Visual examination or comparison with previous examinations is a tedious and time-consuming task. To perform the necessary analyses in the clinical routine, computer assistance is desirable.

Today, diffuse diseases of the lung parenchyma are diagnosed only descriptively. In order to perform follow-up examinations or clinical trials up to current standards, a reproducible, objective, and quantitative evaluation of diffuse diseases of the lung parenchyma is required (9). In addition to a global assessment of a parenchymal disease, its spatial distribution can be of clinical importance. For instance, lung volume reduction surgery (LVRS) has been shown to be signifi-

cantly more effective in cases of heterogeneously distributed emphysema than in patients with a homogeneous distribution (10,11). The degree of deterioration can vary significantly between the left and right lung or between different lobes and segments. A compartment-specific assessment of emphysema is especially desirable in conjunction with recent approaches concerning bronchoscopic LVRS, where air flow to emphysematous segments is blocked by using one-way bronchial valves (12,13).

A method for reproducible 3D identification of lungs, lobes, and segments provides the means to assess regional quantitative parameters for treatment planning and monitoring. Although experienced radiologists might be able to identify lobar and sometimes even segmental boundaries on CT scans, manual delineation on over 300 CT images is unthinkable in the clinical routine. In addition to pure assistance in quantification, computers have to provide support for the radiologist in identifying the lung regions quickly and conveniently. The methods have to work robustly even in cases of severe disease.

By using the region information, functional parameters such as volume, mean lung density, pixel index (14), bulla index, and emphysema type (15) can be extracted for each compartment. This increases the significance of a CT-based prediction of postoperative lung function in cases of resection of a lung, lobe, or segment (16–18), which is standard therapy for patients with primary non–small cell lung cancer. Currently, perfusion scintigraphy is performed in order to obtain a functional prognosis. Since scintigraphy does not allow 3D image analysis, it is difficult to acquire accurate estimates for lobar function, not to mention segmental function. Furthermore, the examination is conducted in addition to CT and lung function tests. By correlating quantitative analysis results with patient-individual 3D lung segment morphology obtained directly from CT data acquired previously for diagnostic reasons, additional scintigraphic examinations might become dispensable.

Medical Background

Emphysema is defined anatomically by permanent, destructive enlargement of airspaces distal to the terminal bronchioles without obvious fibrosis (19). Reduced density and other morphologic parameters are used for quantitative evaluation of the stage of disease. CT images of the lung contain the necessary information in order to obtain objective and quantitative results.

For primary non–small cell lung cancer, the only treatment known to provide a good chance of cure is surgical removal of the tumor. This usually implies resection of the complete lung, lobe, or segment in which the tumor is located (20). Since smoking is known to cause not only lung cancer but also emphysema, the lung function of many resection candidates is already reduced preoperatively. This raises the question of whether the patient will have enough functional lung parenchyma after undergoing lung resection surgery. Preoperative lung function is assessed by measuring the patient's FEV_1 (forced expiratory volume in 1 second) (21,22). Perfusion scintigraphy is the current standard procedure for determination of the distribution of lung function. Evaluation of possible resection strategies such as pneumonectomy or lobectomy is based on the combination of the measured FEV_1 and the predicted percentage of remaining lung function estimated with scintigraphy.

Existing Methods

With the introduction of multidetector CT images, scientific publications concerning the identification of anatomic lung structures emerged. Examples of airway segmentation and analysis methods can be found in references 23–25. Diverse algorithms for automated lung segmentation are presented in references 26–29. Concerning lobar segmentation, a fissure detection and atlas-based algorithm was proposed by Zhang et al (30). Another method based on a Voronoi division of the lungs starting from lobar bronchi was used to identify the lobes by Zhou et al (31).

A method integrating extracted information on both the supply regions and the lobar fissures while providing the means for fast interactive corrections was proposed by Kuhnigk et al (29) and integrated into the described software. For the segmentation of sublobar segments that are not separated by fissures, our approach includes an enhanced version of the algorithm presented by Krass et al (18) in 2000, which uses techniques similar to the lobe segmentation approach proposed in reference 31 in 2003. The refined version makes use of the information provided by the lobar segmentation and needs manual interaction only for quick correction in case of misclassifications of bronchi during the automated preprocessing.

Qualitative and quantitative analyses of the lung parenchyma were proposed in references 14 and 15 and references 32–34. An integration of compartment segmentation methods and quantitative analyses was presented by Reinhardt et al (35) where the fissure-based lobe segmentation from reference 30 was used, not including further segmental subdivision. A CT image–based prediction of postoperative lung function in patients with lung cancer was compared with measured postoperative values (16) and the perfusion scintigraphy prognosis (36) by Wu et al (16,36). The predictions were based on volume measurements only, and the lobes were identified manually in the CT data.

Despite the recent increase in research activities in pulmonary image processing, currently available commercial software does not include the analysis of lung parenchyma in CT images on the basis of lobar or segmental regions.

MeVisPULMO

The application prototype MeVisPULMO allows CT-based functional diagnosis with respect to the anatomic compartments of the lung. It includes the automated segmentation of airways, lungs, and lung lobes and an approximation of the sublobar segments. By providing the means for convenient interactive refinements of the lobar and segmental regions, robustness in patients with severe pathologic alterations is achieved. The analyses allow a convenient, regional assessment of CT parameters of the lung, such as total volume, mean density, pixel index, or bulla index.

MeVisPULMO was implemented using the rapid prototyping platform MeVisLab and runs standalone on Linux or Microsoft Windows workstations with at least 1 GB of random-access memory (RAM).

Work Flow

Although the technological evolution of computer hardware is constantly continuing, analyzing CT images of the lungs is still a time-consuming process. While computers became faster, the amount of data in current chest CT scans increased at a comparable rate. Seamless integration of the analysis of 200–500 CT sections into the clinical work flow is crucial to the clinical acceptance of any method. MeVisPULMO solves this problem by including fully automated preprocessing, which is performed before the radiologist has even seen the data. The automated preprocessing includes segmentation of the airways and lungs, as well as initial segmentation of lung lobes and segments. It takes about 10 minutes on a standard personal computer (PC) with 2 GB of RAM. Since the radiologist's attendance is not required for this procedure, time is not crucial at this point. The fully automated preprocessing procedure stores its results as DICOM (Digital Imaging and Communications in Medicine) images and is fully detachable from the verification and reporting part of the application, allowing a seamless integration as evidence creator into a radiology information system (RIS)–driven work flow concept (IHE [Integrating the Healthcare Enterprise]). In a clinical setting, the preprocessing should run on a dedicated computer and be triggered automatically after the reconstruction of a CT data set is completed.

At the time the radiologist inspects the data, the complete analysis results are available. Since the automatic detection of the lobes and especially the approximation of the segments in CT data from patients with pathologic alterations are not always sufficiently exact, the first thing the radiologist has to do is to verify and eventually refine the segmentation results interactively. After the segmentation is completed, total volume, mean density, pixel index, bulla index, and emphysema type for each lung, lobe, and segment are displayed and written into a structured textual report for documentation purposes. This quantification step takes only a few seconds. For the prediction of postoperative lung function, the physician specifies the location of the tumor to be resected. On the basis of this information and the extracted parameters, the predicted percentage decrease in lung function is computed for each resection strategy. Since all necessary parameters are already available, the report can be updated accordingly with no further delay. This allows the radiologist to communicate the prognostic results to the surgeon.

Two of the methods involved, the lobar segmentation and the segment approximation, require verification and, eventually, interactive refinement of the results proposed by the automatic preprocessing. On the one hand, there are significant benefits from including possibilities for verification and interactive refinement of more complex image processing procedures into the work

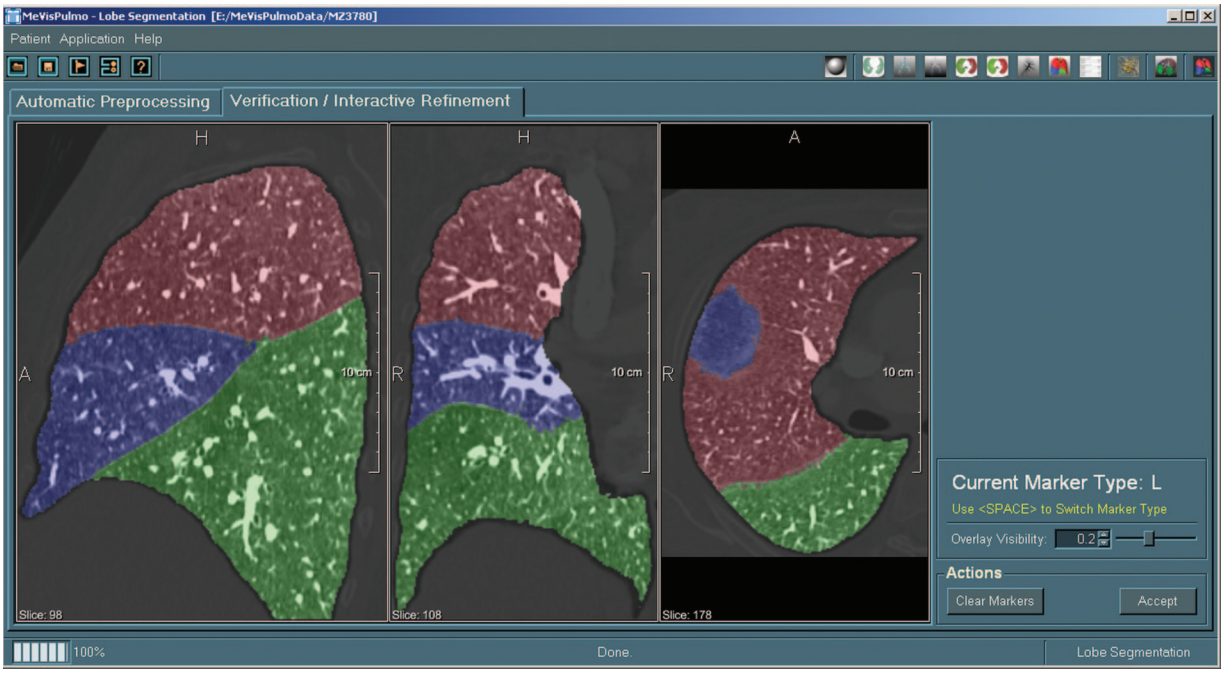

Figure 1. User interface of MeVisPULMO during verification and refinement of the lobar segmentation. The segmented regions are represented by colored overlays on sagittal (left), coronal (middle), and axial (right) images.

flow: The radiologist has actually seen and checked the results that are the basis for all quantitative analyses. This avoids concerns regarding reliability that are often associated with fully automated, nonverifiable approaches. In addition, the possibility of user intervention can make methods applicable even to cases including severe pathologic alterations or anatomic variants. On the other hand, interactive procedures are associated with two possible drawbacks: First, they bring up the issue of reproducibility. There is no guarantee that two analyses performed even on the same data will produce the same results, as would be the case for a fully automated method. Second, they can be extremely time-consuming, and even if the interaction itself is not, the waiting until the modified results are available might be. Depending on the kind of user interaction, the validity of the new results might not be obvious at the point of intervention, so that they have to be verified—and, eventually, modified—again.

Consideration of both the positive and the negative aspects of user interaction had significant influence on the design, implementation, and evaluation of the lobar segmentation procedure. Inter- and intraobserver studies were performed to demonstrate the reproducibility of interactive lobar segmentation. These studies are described in greater detail in the "Evaluation" section. The critical point of integrating the interaction into a clinically acceptable work flow was addressed by ensuring that all time-consuming tasks are already performed during the automatic preprocessing, while the parts possibly requiring user intervention are placed at the end of the processing pipeline. Special algorithms described in greater detail in the "Methods and Algorithms" section allow modifying the segmentation results and verifying the effects of the modifications in real time.

More concretely, the lobar regions computed automatically are indicated by means of color overlays in sagittal, coronal, and axial sections, which can be inspected simultaneously (Fig 1). The lobar regions can be refined iteratively by placing additional markers on blood vessels in any of the views with the mouse. Since each marker impacts not only its local environment but the complete subtree of the selected vessel, few markers (usually one to 10) suffice in order to refine the segmentation results, if necessary at all. The effect of a new marker can be verified immediately due to the instant updating of the colored regions in each of the views. The lobe segmentation verification and refinement procedure takes about 1 minute per lung. Since, as mentioned previously, the regional quantification step is very

fast, the extracted parameters can be updated with respect to the refined lobar regions immediately.

In case a segmental subdivision of the lobes is desired, the refinement step includes verifying and, if necessary, correcting the identification of the segmental bronchi using a 3D surface rendering of the segmented and preclassified bronchial tree (Fig 2). Modifications of the classification can be performed by clicking on a branch and selecting its new designation (for instance, segment 3). Instantly, the color of the subtree distal to the selected branch changes with respect to the new characterization. This procedure can take a few minutes, mostly depending on the abnormality of the patient's airway anatomy. Since, at the present stage of development, the automatic processing is not sufficiently reliable and the work flow of user interaction is not as optimized as for the lobar segmentation, the subdivision of the lobes into the pulmonary segments is probably not yet suited for the clinical routine. However, it does provide important additional functionality in a research setting.

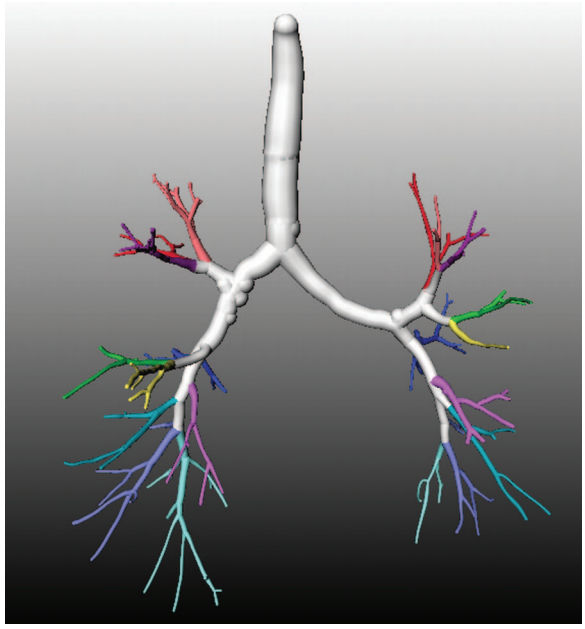

Figure 2. Image produced with 3D surface rendering shows the segmented bronchial tree with color coding of the classified segmental bronchi. Each branch can be selected by using the mouse to change the classification of subtrees manually.

Methods and Algorithms

Segmentation of the Airways.—A seed point in the trachea is found by analyzing two-dimensional rays cast in axial sections. A special region growing method proposed by Selle et al (37) is used for the airway segmentation. It automatically determines an optimal upper threshold from the differential increase of the segmented volume with the increasing threshold interval.

Analysis of the Airways.—The resulting segmented object is analyzed to obtain a graph representation of the bronchial tree describing the branching topology and also including information about the direction, diameter, and length of each branch (37,38).

In order to derive the graph presentation, the tubular structures are skeletonized. The implemented skeletonization method is based on a thinning algorithm and takes special care of anisometric voxel size and boundary noise, yielding exact centerline representations (37). During the erosion process, it is important to check whether the deletion of a particular voxel preserves the 3D topology of the object. For further analysis, the skeleton is interpreted as a graph, where the vertices represent ramification points of the medial axis and the edges represent the parts of the medial axis between the ramifications. Hereby, the skeleton is transformed in a directed acyclic graph with vertices representing branch points and edges representing connections between them. In a postprocessing step, ambiguities are removed from the graph topology, including trifurcations and wrongly assigned groups of branches that are a consequence of noise at the object boundary. A distance transformation evaluates the gradient along and perpendicular to the branches, while the number of voxels assigned to each subgraph indicates the relevance of side branches.

The bronchi belonging to each lung segment are identified automatically. In a first step, the main branches of the tree are evaluated to identify the subtrees belonging to each lobe of the lung. We obtain a fair estimate of the mapping of lung segments to the segmented tree structure by equally dividing the lobar subtrees according to the number of segments in each lobe and by classifying the resulting subtrees according to their relative position. An interactive correction of the resulting anatomic classification is possible. An exemplary analysis result is shown in Figure 2.

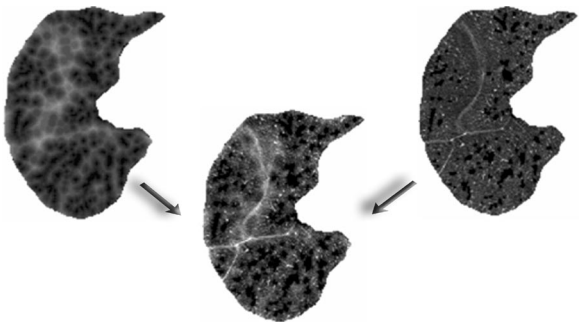

Figure 3. Image showing the vascular distances (left) and original image with the blood vessels masked out (right). Weighted addition of the information from these two images produces a combined image (middle), which allows more robust detection of lobar boundaries.

Segmentation of the Lungs.—Starting from the bronchial tree, a conventional region growing procedure is performed using the fixed threshold interval from −1,024 to −400 HU in order to provide a preliminary mask of the lung parenchyma. Since separate masks for the left and right lung are needed in subsequent processing steps, the bronchi segmentation result is used to block the airway connection between both lungs. Unfortunately, the thoracic airways are not the only obstacle for a lung separation procedure. Emphysematous lungs in particular tend to be inflated by the excessive lung pressure caused by the disease. Therefore, the surfaces of the left and right lung are often in direct contact, resulting in a thin appearance of the separating pleura. Its density is lowered by partial volume effects and usually lies below the upper threshold of −400 HU used for the preliminary segmentation. Therefore, an adaptive threshold method is necessary for region separation. In MeVisPULMO, a marker-based 3D watershed transform (39) restricted to the area of the preliminary lung mask is performed in order to obtain separate masks for each lung robustly. By analyzing the preliminary lung mask, two sets of markers are generated automatically for the watershed operation in order to define left and right lung area. Owing to the threshold constraint during the preliminary segmentation, lung vasculature is excluded by the proposed procedure. Since this is necessary for subsequent image processing, several kernel-based filters including morphologic closing are combined in order to close gaps in the parenchyma masks.

The lung segmentation is described in greater detail in reference 29.

Segmentation of the Lobes.—The guiding principle in our method is to avoid a strict dependence on the existence and visibility of lobar fissures in the patient's lung. While fissure detection algorithms exist (30), a considerable amount of clinical cases show progressive widening, incompleteness, or even absence of a fissure, making robust fissure detection difficult. Nearby tumors, atelectasis, or emphysematous changes can present additional problems for fissure-oriented segmentation algorithms. Hence, instead of explicitly detecting fissures, our algorithm makes use of the absence of larger vessels in proximity to the lobar boundaries. To quantify this absence for computational use, a segmentation of the vasculature is needed. The segmentation of blood vessels can be restricted to the area defined by the previously computed lung masks. Because of the high contrast between blood vessels and parenchyma, a conventional 3D region growing algorithm is sufficient to obtain at least a superset of all larger pulmonary blood vessels. By searching the data for a high-density area in the image region where the hilum is expected, suitable seed points are detected automatically.

In order to quantify the absence or rareness of larger vessels close to the lobar boundaries, a Euclidean distance transform is performed. In other words, the Euclidean distance of each voxel in the lungs to the closest vessel voxel is calculated. An example of a resulting distance map is shown in the left part of Figure 3. Brighter regions indicating greater distances indicate the approximate fissure locations on the distance map. To actually compute the distances, the multidimensional distance transform algorithm for digitized images proposed by Saito and Toriwaki (40) is used. In modern multidetector CT scans, the fissures show at least partially higher density than the surrounding parenchyma (Fig 3, right image). Since the fissure locations are only roughly indicated in the distance map, incorporation of the density information is desirable for a more accurate definition of the lobar boundaries.

Figure 3 shows the effect of the combination of the 3D distance image with the density information on a solitary axial CT section. In the distance image to the left, fissure locations can be estimated visually but appear blurred, whereas in the original image to the right, the fissures can be

traced in more detail where visible but partially show little or no contrast. In the combined image, the thin fissure lines are broadened and, where not visible, roughly continued by the influence of the distance image. This results in a more robust lobar separation in the following segmentation step.

To finally obtain the lobar areas from the preprocessed image, a segmentation method is needed to allow the extraction of 3D-connected components separated by local maxima. Owing to the variety of representations and abnormalities with respect to the lobar anatomy, a convenient way to refine the automated results is desirable. The multidimensional interactive watershed transform (IWT) proposed by Hahn and Peitgen (39) covers both aspects.

The general idea of the watershed algorithm is to separate regions with intermediary areas of local maxima. The IWT in particular combines this feature with the necessary means for interaction: Its internal data representation allows an arbitrary number of markers to be set and evaluated in real time in order to modify the partition of the lung into the different lobes.

Interaction is not mandatory for the lobe segmentation. A set of markers for each lobe is derived automatically from the bronchial tree analysis.

The lobar segmentation is explained in greater detail in reference 29.

Approximation of the Segments.—The approximation of lung segments stems from the segmented and analyzed airway tree: By assigning each lung voxel to the nearest point of the segmented bronchial tree in the same lobe, the anatomic classification of the bronchial tree induces a partition of the lobes into segments. In addition to the bronchial tree, the vessel structure of the arteries can be segmented and analyzed to enhance the accuracy of the approximated positions of segment boundaries. Figure 4 shows the resulting segmental regions by means of colored overlays.

Extraction of Region-specific Functional CT Parameters.—By using the information acquired in the preceding region identification steps, region-specific CT parameters can now be extracted easily from the CT data. Currently, the program assesses the volume, mean density, pixel index, bulla index, and emphysema type of each lung, lobe, and segment. The pixel index (14) is defined as the ratio of lung voxels below a certain threshold (established values are −920 HU or −950 HU) to the total number of voxels in the lung. Its definition implies that the pixel index depends significantly on scan and reconstruction parameters as well as on the patient's respiratory state. In addition, the size distribution of emphysematous lesions is not taken into account.

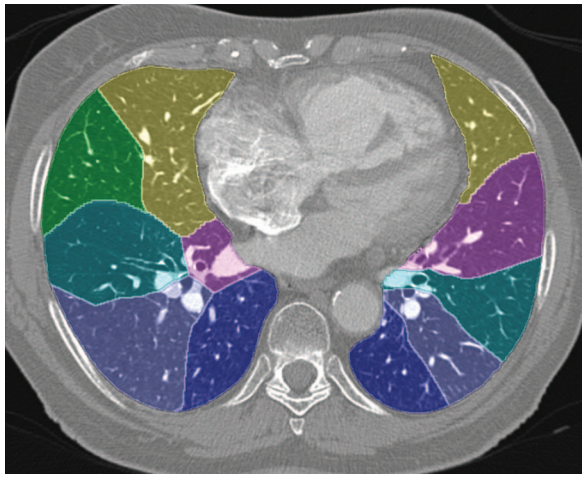

Figure 4. Axial CT image shows the results of estimation of the segments, which are represented by colored overlays with white boundary lines.

The latter aspect in particular is addressed by the parameters bulla index and emphysema type (15). The bulla index is derived from the percentage of areas covered by small, medium, and large bullae, respectively, which in this context are defined as continuous low-attenuation areas. Its values range between 0 and 10, with higher values indicating increased destruction. The emphysema type provides an estimate of whether bullous or small, diffuse lesions dominate. Values are close to +1 in the former case and approach −1 in the latter. A detailed definition of bulla index and emphysema type is given in reference 15.

Prediction of FEV_1.—The basis for a prognosis of postoperative FEV_1 is the distribution of preoperative lung function. A basic assumption of our approach is that by subtracting the contribution of the resected volume from the preoperatively measured lung function, a good estimate of the postoperative value is provided. In cases of lung volume reduction surgery (LVRS) in patients with severe emphysema, functional regions of the parenchyma are given more room for expansion. Hence, lung function is actually supposed to increase after resection of the more emphysematous parts. Since there are no obvious

heuristics for estimating this increase, we have not yet developed a model to predict FEV_1 for LVRS. However, the presented model assumption generally applies in the case of oncologic resections, where emphysema is usually not in its terminal stage. Despite the exclusion of patients with severe emphysema, the distribution of emphysematous lesions can have a significant impact on the prognosis. If the tumor is located in a lung region with relatively (ie, compared to the other parts of the lung) little emphysema, the loss of lung function is expected to be larger than in the case of resection of a more emphysematous region. This aspect was included in the proposed model.

Let R be an arbitrary disjoint partition of the lungs (for instance, the lobar regions). For each region r in R, let $f(r)$ denote the relative functional contribution of r. Therefore, a necessary precondition is given by the following formula:

$$\sum_{r \in R} f(r) = 1.$$

In a first approach, an estimate for the functional contribution of a specific lung region r to the total lung function is given by the region's volumetric contribution $v(r)$ (the volume of region r divided by the total lung volume). Thus, for a volume-based prediction, we define $f(r) := v(r)$. This choice is consistent with the necessary precondition.

The next step is to incorporate information about the spatial distribution of emphysema. A boundary condition for the model is given by the assumption that the prediction equals the volume-based prognosis if the emphysema is distributed exactly homogeneously, in which case it has no influence on the resection strategy. Since the pixel index (PI) parameter is currently more established than bulla index and emphysema type, the extracted region-specific PI measurements are used to introduce information about the spatial distribution of emphysema into our model. As suggested previously, the pixel index is not always a good parameter for comparing emphysema scores acquired from different patients, scans, or reconstructions. However, by correlating PI scores of lung regions from the same scan, a reliable estimate for the spatial distribution of emphysema is obtained. According to the definition of the pixel index given in the preceding section, its values range from 0 to 1 (or from 0% to 100%, respectively).

Since there is no evidence that a more complex relation would be more appropriate, a linear correlation between the inverse of the pixel index ($1 - \mathrm{PI}$) and the functional contribution of a subvolume is assumed. We define $f(r)$ as follows:

$$f(r) := c * [1 - \mathrm{PI}(r)] * v(r),$$

where c represents a normalization factor required to make f fulfill the necessary precondition and is defined as follows:

$$c := \left(\sum_{r \in R} [1 - \mathrm{PI}(r)] * v(r) \right)^{-1}.$$

The relative predicted postoperative lung function for the resection of a region r is computed by subtracting $f(r)$ from 100%.

Evaluation

Overall, the segmentation of airways, lungs, and lung lobes was tested on clinical CT scans of over 150 patients, including many with pathologic findings such as tumors, emphysema, fibrosis, and atelectasis. The images were acquired by multiple clinical partners using different CT scanners and protocols. The z resolution varied between 0.8 mm on a multidetector device and 5 mm on conventional spiral CT scanners, while the x and y resolutions varied from 0.55 mm to 0.9 mm. The proposed segmentation methods were applied successfully to each data set. The quality of the airway segmentation and analysis depended strongly on the z resolution of the images. Automated lobe segmentation was possible only for multidetector scans with a reconstruction increment of at most 2 mm. By using the interactive correction method, the lobes could also be segmented successfully in low-resolution images, although the segmentation was less accurate due to the fact that the lobar fissures do not show significant density contrast in thick-section images. In summary, a lobar analysis of CT parameters was possible for each of the clinical scans.

Preliminary reproducibility studies were conducted on a high-resolution data set (Volume Zoom [Siemens Medical Solutions, Erlangen, Germany]; section thickness, 1.25 mm; voxel size, $0.8 \times 0.8 \times 1.0$ mm), which, apart from an extra fissure and partially disintegrating fissures, showed relatively normal physiology. The studies were performed at a development stage where the automated marker generation was not yet available, forcing each user to place at least one

marker in each lobe manually. An intraobserver study was performed that compared five results produced by the same user, and an interobserver experiment was conducted with the results from five different users. Both studies were performed on the right lung of the selected patient. No restriction on the amount of interaction was applied.

For both studies, the statistical analysis of the segmented lobe volumes showed a standard deviation of well below 1% per lobe. To verify the consistency of the segmentation results more precisely, the similarity measure S was computed for each pair of results as follows: Let L be the number of voxels in the segmented lung and let $cons(R1;R2)$ denote the number of voxels within that lung that are classified consistently by the two segmentations $R1$ and $R2$, then we define the similarity $S(R1;R2)$ as the ratio of the consistent volume and the total lung volume:

$$S(R1;R2) = cons(R1;R2)/L.$$

This similarity measure is also called *Jaccard similarity* (41). Similarities for both the inter- and intraobserver studies were all above 99.5%. Detailed study results can be found in reference 29.

A second trial was conducted that compared the quantitative analysis results of MeVisPULMO and established analysis software (Pulmo [Siemens Medical Solutions]). Thirty multidetector CT data sets (Volume Zoom [Siemens Medical Solutions] and MX 8000 [Philips Medical Systems, Best, the Netherlands]) were analyzed by both tools. Since Pulmo does not support region-specific quantification, the compared parameters volume, mean lung density (MLD), and pixel index (PI) were compared for the whole lung only. Measured correlations for volume, MLD, and PI were 0.997, 0.975, and 0.999, respectively.

The segment approximation method was validated in vitro with two specimens of the left human lung. It was possible to work with high radiation doses, resulting in excellent image quality. The bronchi of the specimens were also recognizable in the peripheral regions of the lung. The bronchial tree was segmented, and the lung segments were determined with the methods described earlier. The trees obtained from the specimens were systematically pruned in five steps in order to simulate the incomplete bronchial trees obtained from in vivo radiologic data. The pruning steps were defined by equal intervals of bifurcation hierarchies.

To validate the approximation methods for the lung segments, the predictions made for the pruned casts and the exact segmental anatomy of the specimens were compared. The measure for the approximation accuracy was the percentage of correctly approximated voxels. The bronchial tree of the specimens could be segmented between three and four generations beyond the segmental bronchi (corresponding to the sixth- or seventh-order bronchi). The segments approximated by using this unpruned bronchial tree were used as reference segments for the validation study. The correctness of the classification of the segmental bronchi was ensured by manual identification by an expert.

The consistency of the segment approximation with the reference was still above 92% after pruning three generations, about 84% after the fourth pruning step, and 70% after the fifth. The quality of the fifth pruning step corresponds to the quality of the segmentation results achieved in the conventional helical CT data sets. The quality of the segmentation results for the multidetector CT data set was very near to that of the fourth pruning step. From this, one can conclude that the accuracy of the segment determination (percentage of correctly approximated voxels) is about 70% when based on conventional helical CT data and more than 80% when based on multidetector CT data. Evaluation results are presented in detail in reference 18.

In order to evaluate the CT-based prognosis of postoperative FEV_1, a trial was set up to show retrospectively that CT-based FEV_1 prediction by using MeVisPULMO correlates significantly with the prognosis of the current standard method, perfusion scintigraphy. Acquisition requirements were a histologically verified diagnosis of bronchial carcinoma, preoperative scintigraphy, and subsequent lobectomy or pneumonectomy. CT data were acquired by using a single-detector spiral CT unit (Somatom Plus 4 [Siemens Medical Solutions]) and reconstructed to 3- and 5-mm section thickness. Overall, 28 perfusion scintigraphy–based predictions, consisting of 15 for lobectomies and bilobectomies and 13 for pneumonectomies, were compared against the CT-based values computed by using MeVisPULMO. The predicted values were compared as percentage of the preoperative FEV_1. The overall correlation was 0.763 with a P value of below .00001. There was no significant systematic deviation between the two procedures (<3%).

Discussion

During the successful analysis of over 150 patient data sets, the proposed software demonstrated its

applicability and robustness with respect to clinical CT. In terms of quantitative evaluation, the lobe segmentation reproducibility study and the accuracy evaluation of the segment approximation method indicate that the image processing results are a reliable basis for the region-specific quantification. The comparison with an established lung analysis tool showed a strong correlation of the extracted parameters while reducing the necessary interaction substantially and providing additional features such as lobar quantification. The first step of clinical evaluation of CT-based FEV_1 prediction, the performed comparison with perfusion scintigraphy–based prognosis, indicates that the correlation of CT with the current standard method is good but not outstanding. The nature of the prediction differences is unclear, since no ground truth was available for the conducted trial.

By allowing a 3D assessment of lung and lobe regions, the CT-based approach has the potential to exceed perfusion scintigraphy in accuracy. A clinical trial is currently being performed in order to compare the CT-based prognosis not only with the prediction by perfusion scintigraphy but also with the measured postoperative FEV_1 on the day of postoperative discharge. Modern scanner hardware (Sensation 16 [Siemens Medical Solutions]) is being used for this trial so that high-resolution images will be available, allowing full exploitation of the advantages of 3D image analysis. This trial might provide evidence about the premises under which CT-based predictions match or even outperform perfusion scintigraphy in accuracy, potentially increasing reliability in predicting postoperative lung function in cases of lung resection planning.

By featuring fully automated identification procedures for all analyses but additionally providing methods for convenient verification and correction of the lung decomposition into lobes and segments, the proposed software allows a simple and robust assessment of established CT parameters specifically for each functional lung component. The accurate region-based extraction of lung function parameters makes it possible to observe and quantify effects distributed unequally across the lungs, thus permitting a more detailed diagnosis and helping in the monitoring of disease progress and treatment.

Acknowledgments: The research that led to the presented results was conducted as part of the cooperation project VICORA (Virtual Institute for Computer Assistance in Clinical Radiology) (*www.vicora.de*). We thank all partners who made this publication possible by their continuous support.

References

1. Rubin GD, Napel S, Leung AN. Volumetric analysis of volumetric data: achieving a paradigm shift. Radiology 1996; 200:312–317.
2. Fuchs TO, Kachelriess M, Kalender WA. System performance of multislice spiral computed tomography. IEEE Eng Med Biol Mag 2000; 19:63–70.
3. Flohr TG, Schoepf UJ, Kuettner A, et al. Advances in cardiac imaging with 16-section CT systems. Acad Radiol 2003; 10:386–401.
4. Ravenel JG, McAdams HP, Remy-Jardin M, Remy J. Multidimensional imaging of the thorax: practical applications. J Thorac Imaging 2001; 16:269–281.
5. Muller NL. Computed tomography and magnetic resonance imaging: past, present and future. Eur Respir J Suppl 2002; 35:3s–12s.
6. Johkoh T, Muller NL, Nakamura H. Multidetector spiral high-resolution computed tomography of the lungs: distribution of findings on coronal image reconstructions. J Thorac Imaging 2002; 17: 291–305.
7. Leppek R, Krass S, Bourquain H, et al. Virtual organization in the digital age of radiology: principle and solution for radiologic research? Rofo Fortschr Geb Rontgenstr Neuen Bildgeb Verfahr 2003; 175:1556–1563.
8. Peitgen HO, Krass S, Lang M. Computer assistance in clinical image-based diagnosis and therapy: a challenge for German research. Rofo Fortschr Geb Rontgenstr Neuen Bildgeb Verfahr 2004; 176:297–301.
9. Bankier AA, De Maertelaer V, Keyzer C, Gevenois PA. Pulmonary emphysema: subjective visual grading versus objective quantification with macroscopic morphometry and thin-section CT densitometry. Radiology 1999; 211:851–858.
10. McKenna RJ Jr, Brenner M, Fischel RJ, et al. Patient selection criteria for lung volume reduction surgery. J Thorac Cardiovasc Surg 1997; 114: 957–964.
11. National Emphysema Treatment Trial Research Group. Patients at high risk of death after lung-volume-reduction surgery. N Engl J Med 2001; 345:1075–1083.
12. Ingenito EP, Reilly JJ, Mentzer SJ, et al. Bronchoscopic volume reduction: a safe and effective alternative to surgical therapy for emphysema. Am J Respir Crit Care Med 2001; 164:295–301.
13. Maxfield RA. New and emerging minimally invasive techniques for lung volume reduction. Chest 2004; 125:777–783.
14. Kalender WA, Rienmueller R, Seissler W, Behr J, Welke M, Fichte H. Measurement of pulmonary parenchymal attenuation: use of spirometric gating with quantitative CT. Radiology 1990; 175: 265–268.
15. Blechschmidt RA, Werthschutzky R, Lorcher U. Automated CT image evaluation of the lung: a morphology-based concept. IEEE Trans Med Imaging 2001; 20:434–442.
16. Wu MT, Chang JM, Chiang AA, et al. Use of quantitative CT to predict postoperative lung function in patients with lung cancer. Radiology 1994; 191:257–262.

17. Shennib H. Sublobar resection for lung cancer. Eur J Cardiothorac Surg 1999; 16(suppl 1):S61–S63.
18. Krass S, Selle D, Boehm D, et al. Determination of bronchopulmonary segments based on HRCT data. In: Lemke HU, Vannier MW, Inamura K, Farman AG, Doi K, eds. Computer assisted radiology and surgery. Amsterdam, the Netherlands: Elsevier, 2000; 584–589.
19. Snider GL. Chronic obstructive pulmonary disease: a definition and implications of structural determinants of airflow obstruction for epidemiology. Am Rev Respir Dis 1989; 140(3 pt 2):S3–S8.
20. Ginsberg RJ, Rubinstein LV. Randomized trial of lobectomy versus limited resection for T1 N0 non-small cell lung cancer: Lung Cancer Study Group. Ann Thorac Surg 1995; 60:615–622.
21. Kearney DJ, Lee TH, Reilly JJ, DeCamp MM, Sugarbaker DJ. Assessment of operative risk in patients undergoing lung resection: importance of predicted pulmonary function. Chest 1994; 105: 753–759.
22. Schulz C, Emslander HP, Riedel M. Risk assessment of patients before lung surgery. Chirurg 1999; 70:664–673.
23. Prêteux F, Fetita C, Grenier P, Capderou A. Modeling, segmentation and caliber estimation of bronchi in high-resolution computerized tomography. J Electronic Imaging 1999; 8:36–45.
24. Tschirren J, Palágyi K, Reinhardt JM, Hoffman EA, Sonka M. Segmentation, skeletonization, and branchpoint matching: a fully automated quantitative evaluation of human intrathoracic airway trees. In: Dohi T, Kikinis R, eds. Lecture notes in computer science 2489. Berlin, Germany: Springer, 2002; 12–19.
25. Aykac D, Hoffman EA, McLennan G, Reinhardt JM. Segmentation and analysis of the human airway tree from three-dimensional x-ray CT images. IEEE Trans Med Imaging 2003; 22:940–950.
26. Hu S, Hoffman EA, Reinhardt JM. Automatic lung segmentation for accurate quantitation of volumetric x-ray CT images. IEEE Trans Med Imaging 2001; 20:490–498.
27. Leader JK, Zheng B, Rogers RM, et al. Automated lung segmentation in x-ray computed tomography. Acad Radiol 2003; 10:1224–1236.
28. Kitasaka T, Mori K, Hasegawa J, Toriwaki J. Automated extraction of the lung area from 3-D chest x-ray CT images based upon the 3-D shape model deformation. In: Lemke HU, Vannier MW, Inamura K, Farman AG, Doi K, eds. Computer assisted radiology and surgery. Amsterdam, the Netherlands: Elsevier, 1999; 194–198.
29. Kuhnigk JM, Hahn HK, Hindennach M, Dicken V, Krass S, Peitgen HO. Lung lobe segmentation by anatomy-guided 3D watershed transform. In: Sonka M, Fitzpatrick JM, eds. Proceedings of SPIE: medical imaging 2003—image processing. Vol 5032. Bellingham, Wash: International Society for Optical Engineering, 2003; 1482–1490.
30. Zhang L, Hoffman EA, Reinhardt JM. Atlas-driven lung lobe segmentation in volumetric x-ray CT images. In: Sonka M, Fitzpatrick JM, eds. Proceedings of SPIE: medical imaging 2003—image processing. Vol 5031. Bellingham, Wash: International Society for Optical Engineering, 2003; 308–319.
31. Zhou X, Kobayashi S, Hayashi T, et al. Lung structure recognition: a further study of thoracic organ recognitions based on CT images. In: Lemke HU, Vannier MW, Inamura K, Farman AG, Doi K, Reiber JHC, eds. Computer aided radiology and surgery. Berlin, Germany: Springer, 2003; 1025–1030.
32. Uppaluri R, Mitsa T, Sonka M, Hoffman EA, McLennan G. Quantification of pulmonary emphysema from lung computed tomography images. Am J Respir Crit Care Med 1997; 156:248–254.
33. Coxson HO, Rogers RM, Whittall KP, et al. A quantification of the lung surface area in emphysema using computed tomography. Am J Respir Crit Care Med 1999; 159:851–856.
34. Hara T, Yamamoto A, Zhou X, et al. Automated volume measurements of pulmonary emphysema on 3-D chest CT images. In: Lemke HU, Vannier MW, Inamura K, Farman AG, Doi K, Reiber JHC, eds. Computer aided radiology and surgery. Berlin, Germany: Springer, 2003; 1043–1048.
35. Reinhardt JM, Guo J, Zhang L, et al. Integrated system for objective assessment of global and regional lung structure. In: Niessen WJ, Viergever MA, eds. Lecture notes in computer science 2208. Berlin, Germany: Springer, 2001; 1384–1385.
36. Wu MT, Pan HB, Chiang AA, et al. Prediction of postoperative lung function in patients with lung cancer: comparison of quantitative CT with perfusion scintigraphy. AJR Am J Roentgenol 2002; 178:667–672.
37. Selle D, Preim B, Schenk A, Peitgen HO. Analysis of vasculature for liver surgical planning. IEEE Trans Med Imaging 2002; 21:1344–1357.
38. Selle D, Peitgen HO. Analysis of the morphology and structure of vessel systems using skeletonization. In: Chen CT, Clough AV, eds. Proceedings of SPIE: medical imaging 2001—physiology and function from multidimensional images. Vol 4321. Bellingham, Wash: International Society for Optical Engineering, 2001; 271–281.
39. Hahn HK, Peitgen HO. IWT—interactive watershed transform: a hierarchical method for efficient interactive and automated segmentation of multidimensional gray-scale images. In: Sonka M, Fitzpatrick JM, eds. Proceedings of SPIE: medical imaging 2003—image processing. Vol 5032. Bellingham, Wash: International Society for Optical Engineering, 2003; 643–653.
40. Saito T, Toriwaki JI. New algorithms for Euclidean distance transformation of an n-dimensional digitized picture with applications. Pattern Recognition 1994; 27:1551–1565.
41. Jaccard P. The distribution of flora in the alpine zone. New Phytologist 1912; 11:37–50.